



# Modifying SnS<sub>2</sub> With Carbon Quantum Dots to Improve Photocatalytic Performance for Cr(VI) Reduction

Weidong Li<sup>1,2†\*</sup>, Jianping Qiu<sup>1†\*</sup>, Haihong Jin<sup>3</sup>, Yuanyuan Wang<sup>4</sup>, Dandan Ma<sup>5</sup>, Xinxiang Zhang<sup>4</sup>, Huayun Yang<sup>2</sup> and Fangyuan Wang<sup>6\*</sup>

<sup>1</sup>Zhejiang Normal University Xingzhi College, Jinhua, China, <sup>2</sup>Hangzhou Normal University Qianjiang College, Hangzhou, China, <sup>3</sup>Zhejiang Hongyi Environmental Protection Technology Co., Ltd., Hangzhou, China, <sup>4</sup>Environmental Engineering Corporation of Zhejiang Province, Hangzhou, China, <sup>5</sup>Zhejiang Tianchuan Environmental Science and Technology Co., Ltd., Hangzhou, China, <sup>6</sup>Zhejiang Normal University, Jinhua, China

## OPEN ACCESS

### Edited by:

Kangle Lv,  
South-Central University for  
Nationalities, China

### Reviewed by:

Hua Yang,  
Lanzhou University of Technology,  
China  
Zafar Hussain Ibupoto,  
University of Sindh, Pakistan

### \*Correspondence:

Weidong Li  
lwd@hznu.edu.cn  
Jianping Qiu  
jianpingqiu@zjnu.edu.cn  
Fangyuan Wang  
jhwfy1188@zjnu.edu.cn

<sup>†</sup>These authors have contributed  
equally to this work

### Specialty section:

This article was submitted to  
Photocatalysis and Photochemistry,  
a section of the journal  
Frontiers in Chemistry

Received: 04 April 2022

Accepted: 12 May 2022

Published: 22 June 2022

### Citation:

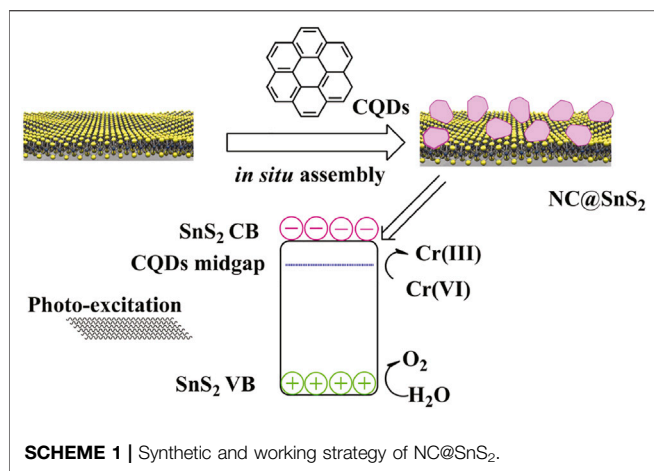
Li W, Qiu J, Jin H, Wang Y, Ma D,  
Zhang X, Yang H and Wang F (2022)  
Modifying SnS<sub>2</sub> With Carbon Quantum  
Dots to Improve Photocatalytic  
Performance for Cr(VI) Reduction.  
Front. Chem. 10:911291.  
doi: 10.3389/fchem.2022.911291

The photoreduction for hazardous Cr(VI) in industrial wastewater has been considered a “green” approach with low-cost and easy-to-go operation. SnS<sub>2</sub> is a promising narrow bandgap photocatalyst, but its low charge carrier separation efficiency should be solved first. In this work, N-doped carbon quantum dots (CQDs) were prepared and loaded onto SnS<sub>2</sub> nanoparticles *via* an *in situ* method. The resulting composite samples (NC@SnS<sub>2</sub>) were characterized, and their photocatalytic performance was discussed. SnS<sub>2</sub> nanoparticles were obtained as hexagonal ones with a bandgap of 2.19 eV. The optimal doping level for NC@SnS<sub>2</sub> was citric acid: urea:SnS<sub>2</sub> = 1.2 mmol:1.8 mmol: 3.0 mmol. It showed an average diameter of 40 nm and improved photocatalytic performance, compared to pure SnS<sub>2</sub>, following a pseudo-first-order reaction with a kinetic rate constant of 0.1144 min<sup>-1</sup>. Over 97% of Cr(VI) was photo-reduced after 30 min. It was confirmed that modification of SnS<sub>2</sub> with CQDs can not only improve the light-harvesting ability but also stimulate the charge separation, which therefore can enhance the photoreactivity of SnS<sub>2</sub> toward Cr(VI) reduction. The excellent stability of NC@SnS<sub>2</sub> indicates that it is promising to be practically used in industrial wastewater purification.

**Keywords:** photocatalyst, SnS<sub>2</sub>, Cr(VI), carbon quantum dots, photoreduction

## INTRODUCTION

Due to the increasing industrial activities, more and more wastewater needs to be treated since it contains heavy metal ions, toxic matters, and hazardous compounds (Lofrano et al., 2013). Among the highly concerned metal ions in industrial wastewater, Cr(VI) attracts public attention since it is easily assimilated by the human body with accumulation effect, exerting harmful effects to the liver. Liver cancer has been related to the excess uptake of Cr(VI). As a consequence, Cr(VI) total amount is listed as one of the quality control quotas for industrial wastewater (Al Nafey et al., 2017). Among the multiple treatment approaches for industrial wastewater, such as water splitting, CO<sub>2</sub> reduction, N<sub>2</sub> fixation, and full adsorption/removal, photoreduction seems like an economic approach with easy-to-go operation and acceptable performance (Santosa et al., 2008; Ji et al., 2015; Shi et al., 2018; Tasbihi et al., 2018; Wang et al., 2018). For example, Sun and coworkers reported the adsorption and removal performance of the yttrium-based metal-organic framework, which allows efficient removal of Sb(VI) in water (Li Q. et al., 2022). Liu and Yang reported a carnation flower-like Bi<sub>2</sub>O<sub>2</sub>CO<sub>3</sub>



photocatalyst for the photoreduction of Cr(VI) (Li L. et al., 2022). Here, with the help of photocatalysts, Cr(VI) is reduced to Cr(III) which is considered less harmful to the human body.

For most reported photocatalysts, high excitation energy in the UV region is required since they are wide bandgap semiconductors. As a consequence, the application of these wide bandgap photocatalysts needs to be assisted by UV-radiation when processing wastewater. To explore narrow bandgap photocatalysts which are expected to be excited by natural solar spectrum, metal sulfide semiconductors have been intensively explored (Azimi and Nezamzadeh-Ejhi, 2015; Xiao and Jiang, 2017; Yan et al., 2017; Li et al., 2018). For example, Lv and coworkers have reported a series of photocatalysts based on Bi<sub>2</sub>O<sub>2</sub>CO<sub>3</sub> and Bi<sub>2</sub>WO<sub>6</sub>/Bi<sub>2</sub>S<sub>3</sub> with visible photoreactivity for NO oxidation and brilliant red X-3B dye (X3B) (Huang et al., 2018; Yang et al., 2019). These works spark the exploration for narrow bandgap photocatalysts. Among these metal sulfide candidates, tin disulfide (SnS<sub>2</sub>) seems attractive due to its perfect spectral matching with solar spectrum, low cost, and more importantly, low bio-toxicity (Cheng et al., 2017). A problem faced by SnS<sub>2</sub>-based semiconductors is their low photocatalytic efficiency. To solve this problem, co-catalysts are doped into SnS<sub>2</sub>, aiming at a higher separation/transportation efficiency of photogenerated charge carriers, so that the photocatalytic efficiency of SnS<sub>2</sub> can be improved (Guo et al., 2016; Jing et al., 2018).

Among the various proposed photosensitizers for photocatalysis, carbon quantum dots (CQDs) have drawn much research attention owing to their virtues of chemical stability, bio-compatibility, economic synthesis, and excellent photoactivity, along with their promising photoelectronic and photocatalytic performance (Zhang et al., 2012; Jiang et al., 2015; Yu et al., 2016). For CQDs smaller than 10 nm, they are composed of sp<sup>2</sup>/sp<sup>3</sup>-hybridized C atoms, with a narrow bandgap covering the whole visible region and even the near-infrared region. In addition, their optoelectronic property, including their bandgap, can be conveniently modified by chemical modifications, offering various kinds of CQDs to meet the requirement for photocatalytic application (Yu et al., 2016).

Guided by the aforementioned consideration, in this work, we intend to prepare N-doped CQDs and modify SnS<sub>2</sub> with these N-doped CQDs. Here, the doped N atoms in CQDs are supposed to offer a midgap for the photogenerated charge carriers in SnS<sub>2</sub> semiconductors, so that the electron mobility can be improved, which promotes the separation and transportation of photogenerated charge carriers. As a consequence, improved photocatalytic efficiency from the resulting composite structure (denoted as NC@SnS<sub>2</sub>) is expected. A schematic presentation for the synthetic strategy of NC@SnS<sub>2</sub> is shown in **Scheme 1**. A full characterization on NC@SnS<sub>2</sub> is performed, and corresponding photocatalytic performance for Cr(VI) photoreduction is discussed as well.

## EXPERIMENTAL DETAILS

### Equipment and Reagents

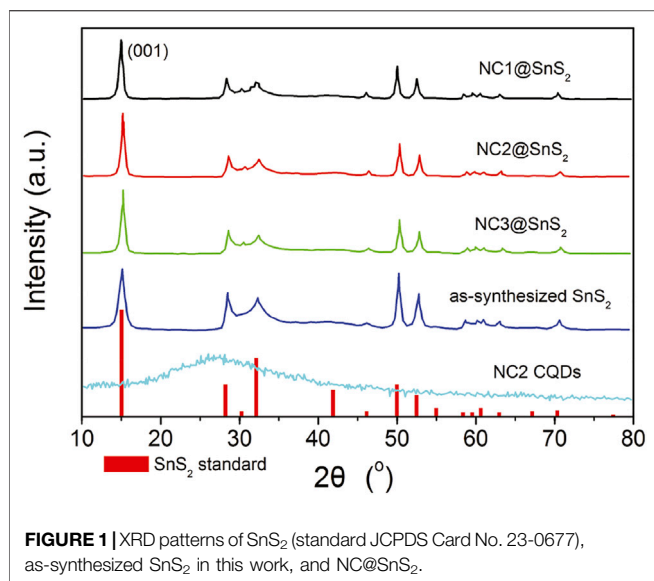
All chemical reagents used in this work were AR-grade ones, including SnCl<sub>4</sub>, thioacetamide (TAA), citric acid (CA), urea (UA), and Nafion. Micromorphology analysis was performed using a Hitachi S4800 (SEM) microscope (Hitachi, Japan), an Oxford X-Max80 field emission scanning electron microscope (JSM-7800, JEOL), a Tecnai F20 (HRTEM), and a Talos F200X (FEI). IR, Raman, and XPS spectra were recorded on a Nicolet iS50 spectrophotometer (KBr method), a Renishaw inVia Raman microscope (excitation = 532 nm), and an ESCALAB250 X-ray Photoelectron spectrometer, respectively. Zeta potentials were determined by electrophoretic light scattering with a zeta sizer (nano series, Malvern, UK). XRD diffraction data were collected on a Rigaku MiniFlex Ultima IV diffractometer (Cu Kα source, λ = 1.5418 Å) with an operating voltage of 40 kV and a current of 15 mA. UV-Vis diffuse reflectance spectra (DRS) were recorded using a Hitachi U-4100 spectrophotometer equipped with an integrating sphere. UV-Vis absorption spectra were obtained using a Hitachi UV-2450 UV-Vis spectrophotometer. Electrochemical parameters were determined by a lock-in-based surface photovoltage (SPV) and an electrochemical workstation (CHI 760E).

### Synthesis of SnS<sub>2</sub> Nanoparticles

SnS<sub>2</sub> nanoparticles were synthesized as follows: a homogeneous solution was prepared by mixing SnCl<sub>4</sub> and TAA with deionized water (molar ratio = 1:3 in 70 ml). This solution was sealed in a Teflon autoclave and heated at 190°C for 6 h. The solid product was separated by centrifugation (×4,000 rpm) and washed by H<sub>2</sub>O/EtOH (1:1). Before usage, the as-synthesized SnS<sub>2</sub> nanoparticles were activated at 60°C for 12 h.

### Synthesis of NC@SnS<sub>2</sub> samples

NC@SnS<sub>2</sub> was synthesized by an *in situ* assembly method described as follows. A homogeneous solution was prepared by mixing CA and UA with deionized water (in 25 ml). The previously obtained SnS<sub>2</sub> nanoparticles (3 mmol) were added and stirred for 30 min (×600 rpm). This suspension was sealed in a Teflon autoclave and heated at 160°C for 4 h. After natural cooling, EtOH (50 ml) was added. The solid product was



separated by centrifugation ( $\times 4,000$  rpm) and washed by H<sub>2</sub>O/EtOH (1:1). The obtained solid powder was dried at 80°C for 12 h and denoted as NC2-1@SnS<sub>2</sub> (CA:UA = 0.30 mmol:0.45 mmol), NC2-2@SnS<sub>2</sub> (CA:UA = 0.50 mmol:0.75 mmol), NC2-3@SnS<sub>2</sub> (CA:UA = 0.90 mmol:1.35 mmol), NC2-4@SnS<sub>2</sub> (CA:UA = 1.2 mmol:1.8 mmol), and NC2-5@SnS<sub>2</sub> (CA:UA = 1.50 mmol:2.25 mmol).

By varying CA:UA ratio, two more NC@SnS<sub>2</sub> samples were synthesized for performance comparison and denoted as NC1@SnS<sub>2</sub> (CA:UA = 1.2 mmol:3.6 mmol) and NC3@SnS<sub>2</sub> (CA:UA = 1.2 mmol:1.2 mmol).

As mentioned in **Section 2.2** and **Section 2.3**, SnS<sub>2</sub> nanoparticles were first prepared as the supporting host; then, a one-step *in situ* assembly method was used to synthesize NC@SnS<sub>2</sub> samples by directly synthesizing/depositing CQDs on SnS<sub>2</sub> surface, as shown in **Scheme 1**, instead of a two-step procedure: preparing CQDs and incorporating them onto SnS<sub>2</sub> nanoparticles. This *in situ* assembly method simplified synthetic operation. In addition, the ratio of CA:UA was changed to modify the N-doping level in NC@SnS<sub>2</sub> (corresponding to NC1@SnS<sub>2</sub>, NC2-4@SnS<sub>2</sub>, and NC3@SnS<sub>2</sub>). By fixing the ratio of CA:UA but changing the total amount of CA and UA, the CQD account in NC@SnS<sub>2</sub> was modified as well (corresponding to the NC2@SnS<sub>2</sub> series). For discussion convenience, CQDs (denoted as NC2 CQDs) were prepared as well, following a similar operation. It can be noticed from the following **Section 2.4** that NC2 CQDs were N-doped ones, aiming at the desired performance.

### Synthesis of Reference Sample: NC2 CQDs

For performance comparison, reference CQDs were synthesized. A homogeneous solution was prepared by mixing CA and UA with deionized water (1.2 mmol:1.8 mmol in 25 ml). This solution was sealed in a Teflon autoclave and heated at 160°C for 4 h. After natural cooling, EtOH (50 ml) was added. The solid product was separated by centrifugation ( $\times 4,000$  rpm) and

washed by H<sub>2</sub>O/EtOH (1:1). The obtained solid powder was dried in a freeze dryer for 2 days and denoted as NC2 CQDs.

### Photocatalytic Performance Evaluation

The photocatalytic performance of NC@SnS<sub>2</sub> samples was performed in a quartz reactor equipped with a cooling accessory via a water bath. The solar spectrum (excitation source) was simulated using a Xe lamp (PLS-SXE 300, 300 W) and a light filter (400 nm cutoff). The reaction temperature was set at 20°C ( $\pm 2^\circ\text{C}$ ). NC@SnS<sub>2</sub> (30 mg) was added into K<sub>2</sub>Cr<sub>2</sub>O<sub>7</sub> aqueous solution (50 mg/L) and treated with an ultrasonic bath for 10 min. Then, this suspension was placed in dark for 2 h to allow full adsorption for photocatalyst. Finally, this mixture was exposed to the solar spectrum. For photoreaction monitoring, 0.3 ml of suspension was extracted each time (time interval = 300 s) and filtered off using a cellulose acetate membrane filter (pore size = 0.22 nm). The resulting solution was treated with diphenylcarbazide (as a chromogenic agent,  $\lambda_{\text{abs}} = 540$  nm) and sent for UV-Vis absorption titration (Qu et al., 2013). Cr(VI) amount was proportional to the absorbance at 540 nm, so its photoreduction percentage was calculated by  $A/A_0$ . Here,  $A_0$  was the initial absorbance value. It was noted that the adsorption of Cr(VI) on the surface of the photocatalyst is negligible (less than 2%), and modification of SnS<sub>2</sub> with CODs has little effect on Cr(VI) adsorption.

The recycling performance of NC@SnS<sub>2</sub> samples was evaluated as follows: after photoreaction, NC@SnS<sub>2</sub> samples were filtered off and washed with plenty of freshwater. After being dried at 80°C for 12 h, the recycled NC@SnS<sub>2</sub> samples were obtained.

### Electrochemical Performance Evaluation

Photo-generated charge transfer behavior was evaluated using an electrochemical workstation (CHI 760E). A three-electrode system was selected, with a Pt wire as the counter electrode, Ag/AgCl (saturated KCl) as the reference electrode, and NC@SnS<sub>2</sub> as the working electrode (surface area = 0.17 cm<sup>2</sup>), using the electrolyte of Na<sub>2</sub>SO<sub>4</sub>, 0.2 M. The working electrode was prepared as follows: A mixture of NC@SnS<sub>2</sub> (50 mg), deionized water (450  $\mu\text{L}$ ), EtOH (500  $\mu\text{L}$ ), and Nafion (5  $\mu\text{L}$ ) was treated with an ultrasonic bath for 10 min. Then, this mixture was spin-coated onto an FTO glass electrode (1.5 cm<sup>2</sup>  $\times$  2.0 cm<sup>2</sup>) and heated at 400°C for 60 min under a pure N<sub>2</sub> atmosphere. Mott-Schottky plots were sampled at 1,000 Hz, 2,000 and 3,000 Hz. Electrochemical impedance spectra (EIS) were recorded at -1.4 V (vs. Ag/AgCl) within 0.1 Hz–10 kHz, using an AC sinusoidal perturbation (10 mV).

## RESULTS AND DISCUSSION

### Morphology and Composition of NC@SnS<sub>2</sub> Samples

As previously mentioned, NC@SnS<sub>2</sub> was prepared by a one-step *in situ* assembly method, where the N atoms in CQDs are supposed to offer a midgap for the photogenerated charge carriers in SnS<sub>2</sub>. This midgap is supposed to improve electron



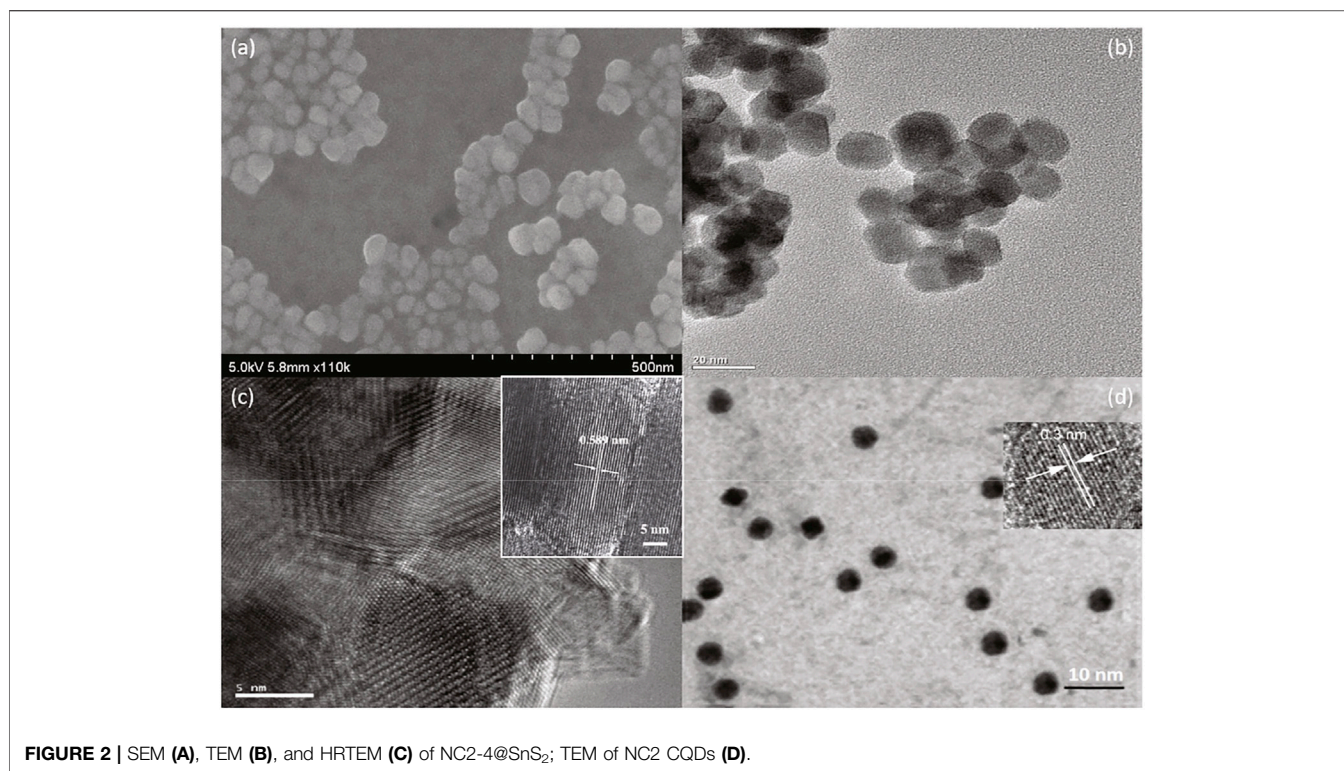


**FIGURE 2** | SEM (A), TEM (B), and HRTEM (C) of NC2-4@SnS<sub>2</sub>; TEM of NC2 CQDs (D).

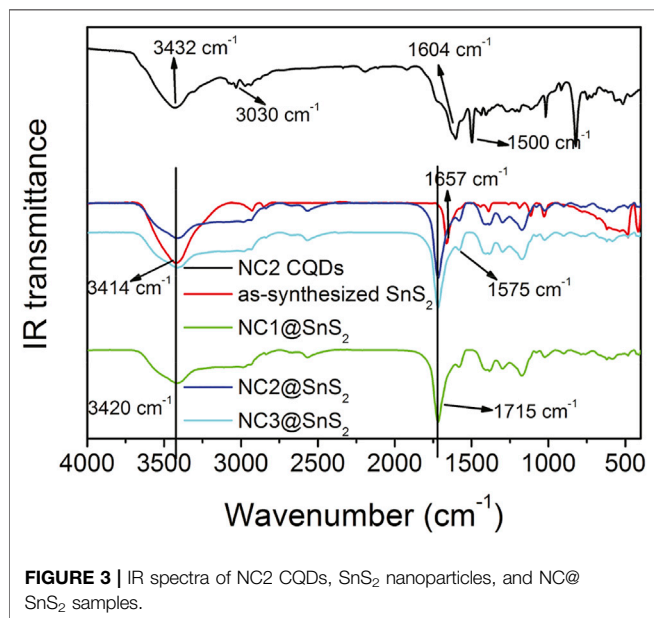
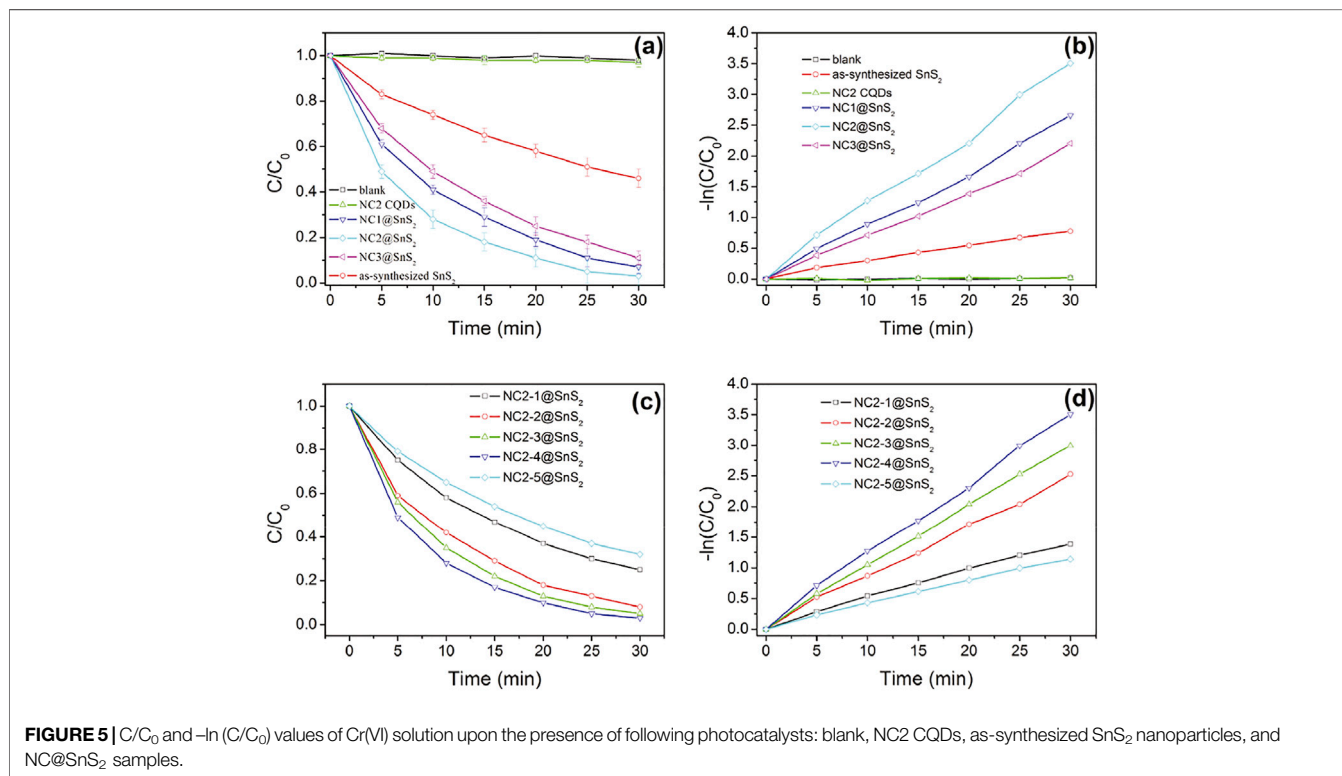
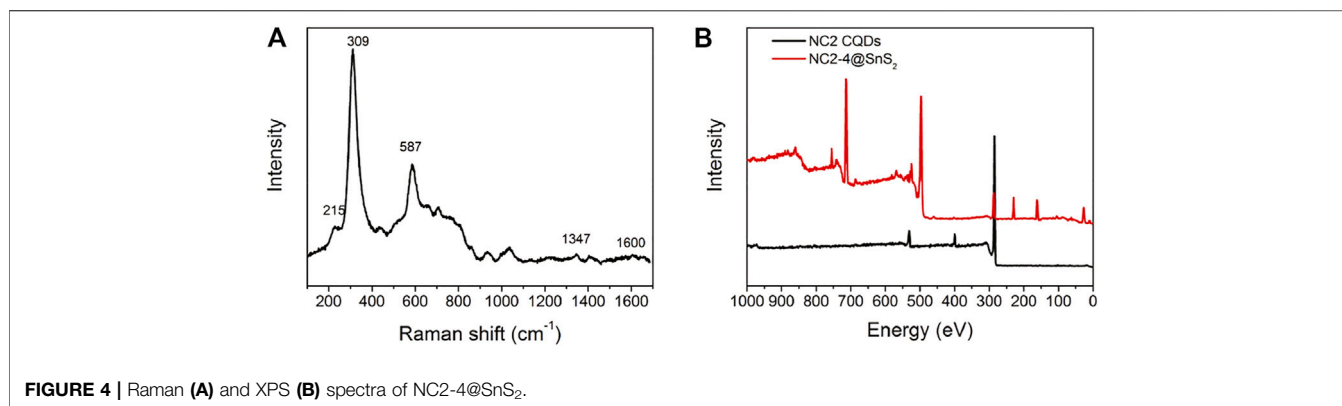


**FIGURE 3** | IR spectra of NC2 CQDs, SnS<sub>2</sub> nanoparticles, and NC@SnS<sub>2</sub> samples.

mobility and thus promote the separation and transportation of photogenerated charge carriers. Simply speaking, here, the active site of NC@SnS<sub>2</sub> should be the N-doped CQDs which capture excited electrons. The successful synthesis and assembly of NC2 CQDs, SnS<sub>2</sub> nanoparticles, and NC@SnS<sub>2</sub> samples are first discussed by comparing their XRD patterns. It is observed from **Figure 1** that the primary diffraction peaks of NC@SnS<sub>2</sub> samples are rather similar to those of as-synthesized SnS<sub>2</sub>

nanoparticles. Sharp diffraction peaks are observed, which confirms the high crystallinity of SnS<sub>2</sub>. All these diffraction peaks shall be indexed to a hexagonal SnS<sub>2</sub> structure (JCPDS Card No. 23-0677). As for NC2 CQDs, a broad diffraction peak with  $2\theta = \sim 27^\circ$  is observed, coming from the highly disordered C atoms (Xia et al., 2016). This broad diffraction peak, however, is not obvious in NC@SnS<sub>2</sub> samples, owing to the low CQDs loading level in them. There is a notable difference in the relative intensity of (001) peak (vs. other diffraction peaks) between NC@SnS<sub>2</sub> and as-synthesized SnS<sub>2</sub> nanoparticles, which means an interaction between NC2 CQDs and SnS<sub>2</sub> that causes variations in crystal size and preferred orientation. It appears that NC@SnS<sub>2</sub> samples tend to grow along the c-axis direction, owing to below two reasons. First, there are enough functional groups on the CQD surface, which allows further nucleation. In addition, SnS<sub>2</sub> nanoparticles tend to aggregate in the presence of NC2 CQDs, which will be confirmed by the following morphology analysis.

The synthesis of NC@SnS<sub>2</sub> was finished by a controllable *in situ* assembly method. Here, NC2 CQDs were synthesized and directly loaded onto SnS<sub>2</sub> nanoparticles under hydrothermal conditions through an electrostatic effect. To confirm the successful *in situ* assembly between SnS<sub>2</sub> host and N-doped CQDs, their zeta potential values are determined as +4.30 mV for the SnS<sub>2</sub> nanoparticles and -9.40 mV for NC2 CQDs (both dispersed in deionized water). There shall be strong electrostatic attraction between SnS<sub>2</sub> host and N-doped CQDs, which leads to an assembly between them. The zeta potential value of a representative NC@SnS<sub>2</sub> sample, NC2-4@SnS<sub>2</sub>, is determined as -4.50 mV, which is close to that of NC2 CQDs (-9.40 mV),



compared to that of SnS<sub>2</sub> nanoparticles (+4.30 mV). This is because SnS<sub>2</sub> nanoparticles are covered by NC2 CQDs whose surface has negative groups such as  $-\text{COO}^-$ . As a consequence, it is concluded that SnS<sub>2</sub> nanoparticles have been successfully covered by NC2 CQDs.

The successful *in situ* assembly is further analyzed via morphological analysis, which gives a visual understanding of NC@SnS<sub>2</sub> samples. Here, the morphology of a representative NC@SnS<sub>2</sub> sample, NC2-4@SnS<sub>2</sub>, is shown in **Figures 2A–C**, including its SEM, TEM, and HRTEM images. The TEM image of NC2 CQDs is shown for comparison (**Figure 2D**). As for NC2-4@SnS<sub>2</sub>, its SEM image suggests that the hexagonal morphology has been well preserved after loading NC2 CQDs. The average diameter of these NC2-4@SnS<sub>2</sub> particles is 40 nm. As

depicted by their TEM and HRTEM images, there are obvious lattice fringes in NC2-4@SnS<sub>2</sub>, with lattice spacing distances of 0.589 and 0.3 nm, respectively. The former one is attributed to the plane (001) from the SnS<sub>2</sub> host. After comparing with the TEM details of NC2 CQDs shown in **Figure 2D**, the latter one is attributed to the plane (002) of graphic carbon from NC2 CQDs (Di et al., 2016; Li et al., 2016). The observation of these lattice fringes on NC2-4@SnS<sub>2</sub> tentatively confirms the successful loading of CQDs on SnS<sub>2</sub> nanoparticles. It is still observed that NC2 CQDs tend to stack on the SnS<sub>2</sub> surface, showing a growth along the *c*-axis (surface vertical direction); this is because the abundant functional groups of NC2 CQDs endow themselves with high affinity for SnS<sub>2</sub> nanoparticles, leading to the stacking along *c*-axis. This morphological analysis is consistent with the

**TABLE 1** | Fitting parameters of the following photocatalysts: blank, NC2 CQDs, as-synthesized SnS<sub>2</sub> nanoparticles, and NC@SnS<sub>2</sub> samples.

Photocatalyst	k (min <sup>-1</sup> )	R <sup>2</sup>
Blank	N/A	N/A
As-synthesized SnS <sub>2</sub>	0.0253	0.997
NC2 CQDs	N/A	N/A
NC1@SnS <sub>2</sub>	0.0869	0.998
NC21@SnS <sub>2</sub>	0.0460	0.998
NC22@SnS <sub>2</sub>	0.0818	0.999
NC23@SnS <sub>2</sub>	0.0991	0.999
NC24@SnS <sub>2</sub>	0.1144	0.998
NC25@SnS <sub>2</sub>	0.0379	0.999
NC3@SnS <sub>2</sub>	0.0711	0.998

above XRD analysis. The *in-situ* assembly of NC2 CQDs on SnS<sub>2</sub> nanoparticles is thus confirmed.

IR technique shall provide more details when analyzing the loading status of CQDs on SnS<sub>2</sub> nanoparticles. IR spectra of NC2 CQDs, SnS<sub>2</sub> nanoparticles, and NC@SnS<sub>2</sub> samples are recorded and compared in **Figure 3**, so that the aforementioned hypothesis about CQDs stacking on SnS<sub>2</sub> can be confirmed. The SnS<sub>2</sub> IR spectrum is a simple one with only several peaks. The broad one around 3,414 cm<sup>-1</sup> is attributed to the vibration of the -OH group (adsorbed water), while the sharp one at 1,657 cm<sup>-1</sup> is attributed to the absorption of unsaturated bonds on the SnS<sub>2</sub> surface (Tan et al., 2016). As for NC2 CQDs, there are several characteristic bands at 3,432 cm<sup>-1</sup>, 3,030 cm<sup>-1</sup>, 1,604 cm<sup>-1</sup>, and 1,500 cm<sup>-1</sup>, which are attributed to the vibrations from -OH (adsorbed water), N-H, C=N, and COO<sup>-</sup> groups (Sun et al., 2013; Tan et al., 2016). After observing the IR spectra of NC@SnS<sub>2</sub> samples, the IR bands from adsorbed water (3,420 cm<sup>-1</sup>) and C=N (1,575 cm<sup>-1</sup>) are still traced. More obviously, the IR band from unsaturated bonds on the SnS<sub>2</sub> surface is blue-shifted to 1715 cm<sup>-1</sup>, compared to that of SnS<sub>2</sub> nanoparticles (1,657 cm<sup>-1</sup>). This spectral shift suggests that the SnS<sub>2</sub> surface has been covered by CQDs, which affects SnS<sub>2</sub> unsaturated bonds and CQDs C=N bonds. Additionally, the IR absorption from CQDs COO<sup>-</sup> groups is not observed in NC@SnS<sub>2</sub> samples, suggesting that these COO<sup>-</sup> groups have been grafted onto the SnS<sub>2</sub> surface.

Raman spectrum is a powerful tool to reveal sample surface chemistry. The Raman spectrum of NC2-4@SnS<sub>2</sub> is shown in **Figure 4A** to get further information about NC@SnS<sub>2</sub> samples. There are intense vibrational peaks of 215 cm<sup>-1</sup>, 309 cm<sup>-1</sup>, and 587 cm<sup>-1</sup>, which are attributed to first-order E<sub>g</sub>, A<sub>1g</sub>, and second-order E<sub>g</sub> of SnS<sub>2</sub>, while those of 1,347 cm<sup>-1</sup> and 1,600 cm<sup>-1</sup> are assigned as the Raman-active graphic (G) and defect (D) bands from CQDs (Muthulingam et al., 2015). In addition, the XPS survey spectra of NC2 CQDs and NC2-4@SnS<sub>2</sub> are shown in **Figure 4B**. As for NC2 CQDs, characteristic peaks from carbon (1s), nitrogen (1s), and O (1s) atoms are clearly observed, which is consistent with the desired elemental composition of NC2 CQDs. After being loaded onto SnS<sub>2</sub> nanoparticles, these peaks are all retrieved from the NC2-4@SnS<sub>2</sub> XPS survey spectrum. In addition, characteristic peaks from Sn (3p<sub>1</sub>, 3p<sub>3</sub>, 3d, 4d) and S (2s, 2p) atoms are observed, confirming the elemental composition of NC2-4@SnS<sub>2</sub>.

Due to the higher electronegativity of nitrogen (3.0) than carbon (2.5), the doped N atoms shall serve as an electron acceptor. This hypothesis is approved by the following analysis on XPS binding energy. As shown by **Supplementary Figures S1A-E** (Supporting Information), the binding energy values of S 2p<sub>1/2</sub> and S 2p<sub>3/2</sub> (162.65 and 161.45 eV) in NC2-4@SnS<sub>2</sub> are decreased by ~0.4 eV, compared to those in SnS<sub>2</sub> nanoparticles. Similarly, the N 1s binding energy values of C-N (400.98 eV) and C=N (401.97 eV) in NC2-4@SnS<sub>2</sub> are smaller than those in NC2 CQDs. The XPS peaks from C=O, C-OH, and C-O-O groups have been weakened or minimized in NC2-4@SnS<sub>2</sub>, compared to those in NC2 CQDs (**Supplementary Figures S1B,C**, Supporting Information), suggesting that these oxygen-containing groups are bonded with Sn. This statement is supported by the Sn binding energy analysis (**Supplementary Figures S1E**, Supporting Information). The binding energy values of Sn 3d<sub>5/2</sub> and 3d<sub>3/2</sub> in SnS<sub>2</sub> nanoparticles are 487.1 and 495.5 eV. In NC2-4@SnS<sub>2</sub>, these values are decreased to 486.7 and 495.2 eV, indicating an interaction between NC2 CQDs and SnS<sub>2</sub>. The composite structure of NC@SnS<sub>2</sub> is thus finally confirmed, where N-doped CQDs and hexagonal SnS<sub>2</sub> crystals have been both identified. With the inserted midgap from CQDs, electron mobility is supposed to be improved, which promotes the separation and transportation of photogenerated charge carriers. Improved photocatalytic performance is thus expected from NC@SnS<sub>2</sub>.

## Photoreduction Performance of NC@SnS<sub>2</sub> Samples

Based on the above analysis and discussion, the successful synthesis of NC@SnS<sub>2</sub> photocatalyst was confirmed. An improved photocatalytic performance was expected from NC@SnS<sub>2</sub>. Here, the photoreduction performance of NC@SnS<sub>2</sub> samples was evaluated via Cr(VI) photoreaction. Photocatalytic performance comparison between NC@SnS<sub>2</sub> samples, having different CQD amounts and different N doping levels was performed, with NC2 CQDs and as-synthesized SnS<sub>2</sub> nanoparticles as reference groups. Here, diphenylcarbazine was used as a chromogenic agent, forming a purple-red compound in an acidic solution with absorption at 540 nm. Cr(VI) amount was proportional to the absorbance at 540 nm, so its photoreduction percentage ( $C/C_0$ ) was calculated by  $A/A_0$ , where  $A_0$  was the initial absorbance value (Qu et al., 2013). It is observed from **Figures 5A,B** that the  $C/C_0$  value of pure Cr(VI) solution remains nearly constant (around 1.0) within the reaction time region 0-30 min, which means that Cr(VI) self-reduction is slim and neglectable. The existence of NC2 CQDs leads to a rather slim decrease ( $C/C_0 = 0.97$  at 30 min). Although NC2 CQDs have intense and broad absorption in the visible region (400–800 nm), the absorbed photons and their energy are wasted by thermal vibration, instead of participating in Cr(VI) photoreduction, which may be caused by the low efficiency of charge separation and transfer. An obvious Cr(VI) photoreduction is observed for as-synthesized SnS<sub>2</sub> nanoparticles ( $C/C_0 = 0.46$  at 30 min). As for NC@SnS<sub>2</sub> samples, their Cr(VI) photoreduction percentage is further



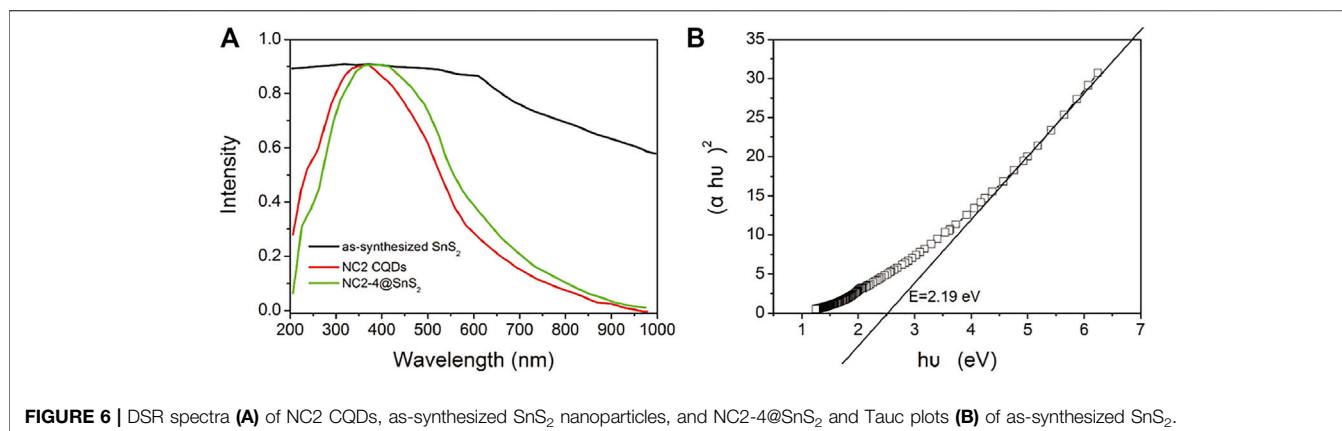


**FIGURE 6** | DSR spectra (A) of NC2 CQDs, as-synthesized SnS<sub>2</sub> nanoparticles, and NC2-4@SnS<sub>2</sub> and Tauc plots (B) of as-synthesized SnS<sub>2</sub>.

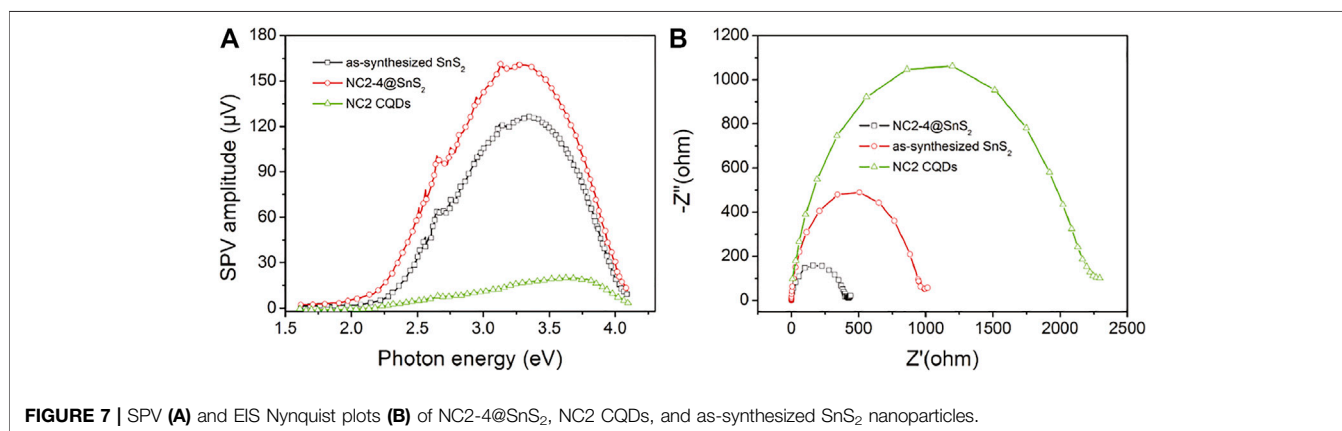


**FIGURE 7** | SPV (A) and EIS Nyquist plots (B) of NC2-4@SnS<sub>2</sub>, NC2 CQDs, and as-synthesized SnS<sub>2</sub> nanoparticles.

increased, with  $C/C_0 = 0.03$  at 30 min for NC2-4@SnS<sub>2</sub>, for example. It is assumed that the conjugation planes in CQDs may accept the excited electrons from SnS<sub>2</sub>, which limits the recombination of photo-induced electron-hole pairs and thus improves the charge transfer separation efficiency of SnS<sub>2</sub>.

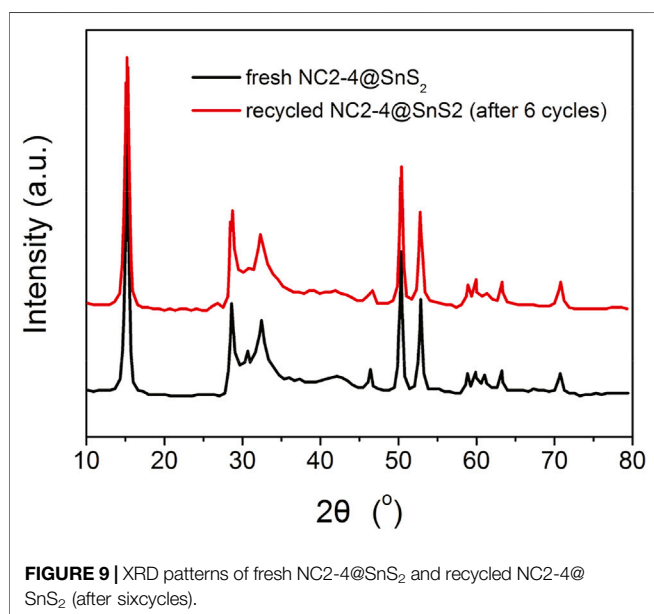
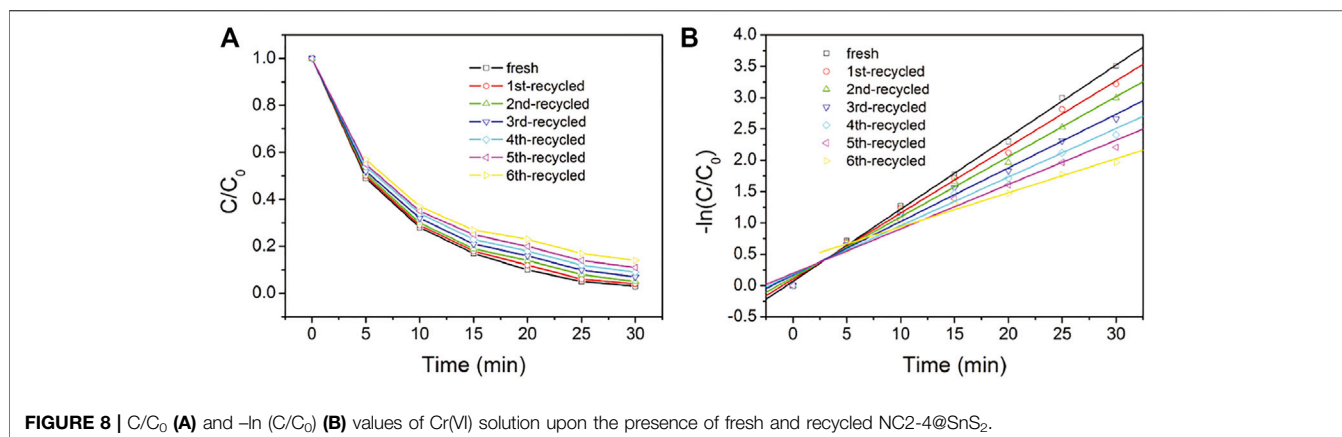
Based on the previous hypothesis, it is assumed that a suitable amount of CQDs with an optimal N doping level, which ensures an efficient electron capture, is required for optimal photocatalytic performance. This statement is supported by the photocatalytic performance comparison between NC@SnS<sub>2</sub> samples with different CQD amounts and different N doping levels, as shown in **Figures 5C,D**. With more (NC1@SnS<sub>2</sub>) or less (NC1@SnS<sub>2</sub>) N-doping level in NC@SnS<sub>2</sub>, compared to NC2@SnS<sub>2</sub>, the photocatalytic performance is simultaneously weakened. This is because N atoms in CQDs help the electron capture procedure and accelerate charge carrier separation. On the other hand, the excess N atoms in CQDs may affect the CQDs conjugation plane and compromise charge carrier separation. As a consequence, there will be an optimal N-doping level, with strong enough electron capture and limited influence on the integrality of the CQD conjugation plane.

Even with the same N-doping level in NC2@SnS<sub>2</sub> samples (NC2-1@SnS<sub>2</sub>, NC2-2@SnS<sub>2</sub>, NC2-3@SnS<sub>2</sub>, NC2-4@SnS<sub>2</sub>, and NC2-5@SnS<sub>2</sub>), their photocatalytic performance is different from

each other, which means that the CQD amount plays an important role as well. Generally speaking, the photocatalytic performance of NC2@SnS<sub>2</sub> is improved with increasing CQD amount. This observation is consistent with the aforementioned statement that CQDs help the electron capture procedure and accelerate charge carrier separation. Yet, NC2-5@SnS<sub>2</sub> shows the worst photocatalytic performance among NC2@SnS<sub>2</sub> samples, although its CQD amount is the highest. This observation is explained by the weakened light harvest since the excess CQDs may worsen SnS<sub>2</sub> light absorption and thus compromise the generation of photo-induced electron-hole pairs. Apparently, the generation of photo-induced electron-hole pairs is controlled by SnS<sub>2</sub> light harvest, not CQD light harvest. Excitation light shall first penetrate CQDs before reaching SnS<sub>2</sub> and being absorbed by SnS<sub>2</sub>. In other words, SnS<sub>2</sub> light harvest is limited by the outer CQDs, which denies a further photocatalytic efficiency improvement. This is a defect for the NC@SnS<sub>2</sub> composite structure.

For a better understanding of the photoreduction dynamics of NC@SnS<sub>2</sub> samples,  $C/C_0$  against reaction time is analyzed by a pseudo-first-order reaction, as described by **Eq. 1**, where  $k$  is the kinetic rate constant and  $t$  is reaction time:

$$\ln(C/C_0) = kt. \quad (1)$$



The detailed fitting parameters are listed in **Table 1**. Good linear fitting is observed. The  $k$ -value of NC2-4@SnS<sub>2</sub> is the highest one among NC@SnS<sub>2</sub> samples.

## Photoreduction Mechanism of NC@SnS<sub>2</sub> Samples

After demonstrating the photoreduction performance of NC@SnS<sub>2</sub> samples, their mechanism is discussed via their UV-Vis diffuse reflectance spectra (DRS), as shown in **Figure 6A**. As for NC2 CQDs, a broad and intense absorption band covering UV and visible region from 200 to 800 nm is observed, with no vibronic progressions or secondary peaks, corresponding to  $p$ - $p^*$  transitions of aromatic C=C bonds, admixed with  $n$ - $p^*$  transitions of C=O bonds (Liang et al., 2013; Di et al., 2015). Regardless of the strong absorption of NC2 CQDs, their photocatalytic performance is neglectable, as mentioned previously, since there are numerous quenching centers in

CQDs ( $-\text{COO}^-$ , for example). As for the as-synthesized SnS<sub>2</sub>, a broad but weak absorption band covering the whole UV-Vis region (200–1,000 nm) is observed, which shall be attributed to the intrinsic band-to-band transitions in SnS<sub>2</sub>. After loading CQDs, NC@SnS<sub>2</sub> DRS shows basically the DRS character of NC2 CQDs, with an obvious red shift of  $\sim 25$  nm. The close contact between NC2 CQDs and SnS<sub>2</sub>, as confirmed previously, shall neutralize the quenching centers in CQDs, which makes CQDs a photosensitizer with a midgap for SnS<sub>2</sub>, showing the aforementioned absorption redshift (Ran et al., 2015; Zhou et al., 2018). Upon photoexcitation of SnS<sub>2</sub>, the excited electrons can be trapped by this midgap level, which facilitates charge carrier transportation and depresses their recombination. As a consequence, an improved photocatalytic performance is observed for CQD-modified SnS<sub>2</sub>.

It has been reported that SnS<sub>2</sub> has a direct bandgap structure; thus, its bandgap ( $E$ ) is calculated by Tauc plots (Kubelk–Munk method), as described in **Eq. 2** (Niu et al., 2014; Zhang et al., 2017):

$$\alpha h\nu = B(h\nu - E)^{1/2}. \quad (2)$$

Here,  $\alpha$  is the absorption coefficient,  $h$  is the Planck constant,  $\nu$  is frequency, and  $B$  is the fitting constant. With the DRS data on hand, the  $E$  value of SnS<sub>2</sub> is calculated as 2.19 eV, as shown in **Figure 6B**. Since the conduction band (CB) level of SnS<sub>2</sub> has been determined as  $-0.19$  eV (against RHE), the valence band (VB) level can be calculated as 2.00 eV (Guo et al., 2018). When SnS<sub>2</sub> is excited, its electron is transferred from VB to CB, resulting in a hole in VB and an excited electron in CB. The excited electron shall be captured by CQDs and then transferred to Cr(VI) to finish the photoreduction. As for the hole in VB, it shall be quenched by H<sub>2</sub>O, with molecular oxygen generated. This proposed mechanism is presented in **Supplementary Figure S2** (Supporting Information).

To strengthen the previous statement, surface photovoltage (SPV) and electrochemical impedance spectra (EIS) of NC2-4@SnS<sub>2</sub>, NC2 CQDs, and as-synthesized SnS<sub>2</sub> nanoparticles are compared in **Figure 7A**. It is obvious that the onset energy of NC2-4@SnS<sub>2</sub> (1.85 eV) is lower than those of NC2 CQDs (2.30 eV) and as-synthesized SnS<sub>2</sub> nanoparticles (2.05 eV),



indicating that NC2 CQDs decrease NC2-4@SnS<sub>2</sub> excitation energy, which is consistent with the finding of their DRS comparison. Higher SPV values are observed for NC2-4@SnS<sub>2</sub> (maximum = 161 μV) within photon energy region 2.25–3.75 eV, compared to those of NC2 CQDs (maximum = 21 μV) and as-synthesized SnS<sub>2</sub> nanoparticles (maximum = 128 μV), which means that NC2 CQDs facilitate the charge carrier separation in NC2-4@SnS<sub>2</sub>. Meanwhile, the smallest radius is observed for the NC2-4@SnS<sub>2</sub> EIS Nyquist plot, among the radii of NC2 CQDs and as-synthesized SnS<sub>2</sub> nanoparticles, as shown in **Figure 7B**. It is thus confirmed that NC2 CQDs show the highest charge carrier separation efficiency, owing to the incorporation of CQDs, which favors Cr(VI) photoreduction. The positive effect of N-doped CQDs on improving the photocatalytic performance of NC@SnS<sub>2</sub> is thus finally confirmed here.

## Recyclability and Durability Performance

The recyclability and durability performance of NC2-4@SnS<sub>2</sub> is then discussed as follows: **Figure 8** shows the photocatalytic performance of recycled NC2-4@SnS<sub>2</sub>. It is observed that the photocatalytic performance has been well preserved after the first five cycles, and then the photoreduction efficiency tends to decrease. Nevertheless, as shown in **Figure 9**, the XRD peaks of recycled NC2-4@SnS<sub>2</sub> (after 6 cycles) are nearly identical to those of fresh NC2-4@SnS<sub>2</sub>, with no obvious shifts or intensity variations. As a consequence, the decreased photoreduction efficiency may be explained by the desorption of CQDs from NC2-4@SnS<sub>2</sub>. Considering that there is only Van der Waals' force, instead of strong chemical bonds, between CQDs and SnS<sub>2</sub>, it is highly possible that the CQDs are extracted and removed from the SnS<sub>2</sub> surface, leading to decreased photoreduction efficiency. A down-bending tendency is observed for the recycled NC2-4@SnS<sub>2</sub>, especially for the sixth-recycled NC2-4@SnS<sub>2</sub>, which tentatively confirms the desorption of CQDs from NC2-4@SnS<sub>2</sub>.

## CONCLUSION

In conclusion, N-doped carbon quantum dots (CQDs) were prepared and loaded onto SnS<sub>2</sub> nanoparticles via an *in situ* method. The resulting composite samples (NC@SnS<sub>2</sub>) were characterized by means of XRD, zeta potential, SEM/TEM, IR, Raman, and XPS to confirm their composite structure. Various N-doping levels and doping amounts were tried to optimize photocatalytic performance. The optimal NC@SnS<sub>2</sub> showed improved photocatalytic performance, compared to pure SnS<sub>2</sub>, following a pseudo-first-order reaction with a kinetic rate constant of 0.1144 min<sup>-1</sup>. It was confirmed by diffuse reflectance spectra, surface photovoltage, and electrochemical impedance spectra that the loaded CQDs increased the charge carrier separation efficiency of SnS<sub>2</sub>.

Good durability was observed for NC@SnS<sub>2</sub>, with at least five full cycles. On the other hand, the charge carrier separation efficiency of NC2-4@SnS<sub>2</sub> is still yet to be satisfied. For further efforts, the holes in SnS<sub>2</sub> VB shall be neutralized quickly to improve charge carrier separation efficiency. In addition, the loaded CQDs served only as a midgap for SnS<sub>2</sub> but showed no contribution to SnS<sub>2</sub> absorption. The intrinsic absorption of SnS<sub>2</sub> should be enhanced to improve its absorption of excitation light. Finally, the durability of NC@SnS<sub>2</sub> should be improved as well. Our primitive suggestion is to replace N-doped CQDs (carbon quantum dots) with N/P-codoped CQDs (Pan et al., 2022). It has been reported that P atoms have a conjugation interaction with SnS<sub>2</sub> (forming Sn <  $\begin{matrix} S \\ S \end{matrix}$  > P structure) (Li, 2001; Yang et al., 2018). In this case, the bonding between CQDs and SnS<sub>2</sub> shall be increased, hoping to get a better durability.

## DATA AVAILABILITY STATEMENT

The original contributions presented in the study are included in the article/**Supplementary Material**; further inquiries can be directed to the corresponding authors.

## AUTHOR CONTRIBUTIONS

WL: supervision and writing and reviewing; JQ: supervision and writing and reviewing; HJ: data acquisition; YW: data acquisition; DM: data acquisition; XZ: data acquisition; HY: data acquisition; FW: supervision.

## FUNDING

The research is supported by the Public Welfare Technology Application Research Project of Zhejiang Province, China (No. LGF22B070001), the Zhejiang Province Natural Science Foundation of China (No. LQ15E080007), the Emerging Talent Program of Zhejiang Province, China (No. 2021R426059), the Jinhua Science and Technology Plan Project (Nos. 2020-4-195 and 2019-4-168), the Competitive Projects in Science and Technology Programmes of Quzhou City (No. 2020K08), the Science Foundation of Qianjiang College (No. 2022QJL06), and the Science Foundation of Qianjiang College and Meiya Company's Project.

## SUPPLEMENTARY MATERIAL

The Supplementary Material for this article can be found online at: <https://www.frontiersin.org/articles/10.3389/fchem.2022.911291/full#supplementary-material>

## REFERENCES

- Al Nafey, A., Addad, A., Sieber, B., Chastanet, G., Barras, A., Szunerits, S., et al. (2017). Reduced Graphene Oxide Decorated with Co<sub>3</sub>O<sub>4</sub> Nanoparticles (rGO-Co<sub>3</sub>O<sub>4</sub>) Nanocomposite: A Reusable Catalyst for Highly Efficient Reduction of 4-nitrophenol, and Cr(VI) and Dye Removal from Aqueous Solutions. *Chem. Eng. J.* 322, 375–384. doi:10.1016/j.cej.2017.04.039
- Azimi, S., and Nezamzadeh-Ejehieh, A. (2015). Enhanced Activity of Clinoptilolite-Supported Hybridized PbS-CdS Semiconductors for the Photocatalytic Degradation of a Mixture of Tetracycline and Cephalixin Aqueous Solution. *J. Mol. Catal. A Chem.* 408, 152–160. doi:10.1016/j.molcata.2015.07.017
- Cheng, Z., Wang, F., Shifa, T. A., Jiang, C., Liu, Q., and He, J. (2017). Efficient Photocatalytic Hydrogen Evolution via Band Alignment Tailoring: Controllable Transition from Type-I to Type-II. *Small* 13, 1702163. doi:10.1002/smll.201702163
- Di, J., Xia, J., Ge, Y., Li, H., Ji, H., Xu, H., et al. (2015). Novel Visible-Light-Driven CQDs/Bi<sub>2</sub>WO<sub>6</sub> Hybrid Materials with Enhanced Photocatalytic Activity toward Organic Pollutants Degradation and Mechanism Insight. *Appl. Catal. B Environ.* 168–169, 51–61. doi:10.1016/j.apcatb.2014.11.057
- Di, J., Xia, J., Ji, M., Wang, B., Yin, S., Xu, H., et al. (2016). Carbon Quantum Dots Induced Ultrasmall BiOI Nanosheets with Assembled Hollow Structures for Broad Spectrum Photocatalytic Activity and Mechanism Insight. *Langmuir* 32, 2075–2084. doi:10.1021/acs.langmuir.5b04308
- Guo, Q., Li, H., Zhang, Q., and Zhang, Y. (2018). Fabrication, Characterization and Mechanism of a Novel Z-Scheme Ag<sub>3</sub>PO<sub>4</sub>/NG/polyimide Composite Photocatalyst for Microcystin-LR Degradation. *Appl. Catal. B Environ.* 229, 192–203. doi:10.1016/j.apcatb.2018.02.023
- Guo, S., Li, X., Zhu, J., Tong, T., and Wei, B. (2016). Au NPs@MoS<sub>2</sub>Sub-Micrometer Sphere-ZnO Nanorod Hybrid Structures for Efficient Photocatalytic Hydrogen Evolution with Excellent Stability. *Small* 12, 5692–5701. doi:10.1002/smll.201602122
- Huang, T., Li, Y., Wu, X., Lv, K., Li, Q., Li, M., et al. (2018). In-Situ Transformation of Bi<sub>2</sub>WO<sub>6</sub> to Highly Photoreactive Bi<sub>2</sub>WO<sub>6</sub>@Bi<sub>2</sub>S<sub>3</sub> Nanoplate via Ion Exchange. *Chin. J. Catal.* 39, 718–727. doi:10.1016/s1872-2067(17)62913-9
- Ji, M., Su, X., Zhao, Y., Qi, W., Wang, Y., Chen, G., et al. (2015). Effective Adsorption of Cr(VI) on Mesoporous Fe-Functionalized Akadama Clay: Optimization, Selectivity, and Mechanism. *Appl. Surf. Sci.* 344, 128–136. doi:10.1016/j.apsusc.2015.03.006
- Jiang, K., Sun, S., Zhang, L., Lu, Y., Wu, A., Cai, C., et al. (2015). Red, Green, and Blue Luminescence by Carbon Dots: Full-Color Emission Tuning and Multicolor Cellular Imaging. *Angew. Chem. Int. Ed.* 54, 5360–5363. doi:10.1002/anie.201511193
- Jing, L., Xu, Y., Chen, Z., He, M., Xie, M., Liu, J., et al. (2018). Different Morphologies of SnS<sub>2</sub> Supported on 2D g-C<sub>3</sub>N<sub>4</sub> for Excellent and Stable Visible Light Photocatalytic Hydrogen Generation. *ACS Sustain. Chem. Eng.* 6, 5132–5141. doi:10.1021/acssuschemeng.7b04792
- Li, D., Yu, S.-H., and Jiang, H.-L. (2018). From UV to Near-Infrared Light-Responsive Metal-Organic Framework Composites: Plasmon and Upconversion Enhanced Photocatalysis. *Adv. Mat.* 30, 1707377. doi:10.1002/adma.201707377
- Li, G., Su, R., Rao, J., Wu, J., Rudolf, P., Blake, G. R., et al. (2016). Band Gap Narrowing of SnS<sub>2</sub> Superstructures with Improved Hydrogen Production. *J. Mat. Chem. A* 4, 209–216. doi:10.1039/c5ta07283b
- Li, L., Gao, H., Liu, G., Wang, S., Yi, Z., Wu, X., et al. (2022). Synthesis of Carnation Flower-Like Bi<sub>2</sub>O<sub>2</sub>CO<sub>3</sub> Photocatalyst and its Promising Application for Photoreduction of Cr(VI). *Adv. Powder Technol.* 33, 103481. doi:10.1016/j.apt.2022.103481
- Li, N. (2001). Synthesis and Characterization of Surface Modified SnS<sub>2</sub> Nanoparticles. *J. Jilin Inst. Chem. Technol.* 18, 7. doi:10.3969/j.issn.1007-2853.2001.02.003
- Li, Q., Li, R., Ma, X., Zhang, W., Sarkar, B., Sun, X., et al. (2022). Efficient Removal of Antimonate from Water by Yttrium-Based Metal-Organic Framework: Adsorbent Stability and Adsorption Mechanism Investigation. *Colloids Surfaces A Physicochem. Eng. Aspects* 633, 127877. doi:10.1016/j.colsurfa.2021.127877
- Liang, Q., Ma, W., Shi, Y., Li, Z., and Yang, X. (2013). Easy Synthesis of Highly Fluorescent Carbon Quantum Dots from Gelatin and Their Luminescent Properties and Applications. *Carbon* 60, 421–428. doi:10.1016/j.carbon.2013.04.055
- Lofrano, G., Meriç, S., Zengin, G. E., and Orhon, D. (2013). Chemical and Biological Treatment Technologies for Leather Tannery Chemicals and Wastewaters: A Review. *Sci. Total Environ.* 461–462, 265–281. doi:10.1016/j.scitotenv.2013.05.004
- Muthulingam, S., Bae, K. B., Khan, R., Lee, I.-H., and Uthirakumar, P. (2015). Improved Daylight-Induced Photocatalytic Performance and Suppressed Photocorrosion of N-Doped ZnO Decorated with Carbon Quantum Dots. *RSC Adv.* 5, 46247–46251. doi:10.1039/c5ra07811c
- Niu, P., Yang, Y., Yu, J. C., Liu, G., and Cheng, H.-M. (2014). Switching the Selectivity of the Photoreduction Reaction of Carbon Dioxide by Controlling the Band Structure of a g-C<sub>3</sub>N<sub>4</sub> Photocatalyst. *Chem. Commun.* 50, 10837. doi:10.1039/c4cc03060e
- Pan, Y., Wei, Z., Ma, M., Zhang, X., Chi, Z., He, Y., et al. (2022). Broadened Optical Absorption, Enhanced Photoelectric Conversion and Ultrafast Carrier Dynamics of N, P Co-Doped Carbon Dots. *Nanoscale* 14, 5794–5803. doi:10.1039/d2nr00211f
- Qu, D., Zheng, M., Du, P., Zhou, Y., Zhang, L., Li, D., et al. (2013). Highly Luminescent S, N Co-Doped Graphene Quantum Dots with Broad Visible Absorption Bands for Visible Light Photocatalysts. *Nanoscale* 5, 12272. doi:10.1039/c3nr04402e
- Ran, J., Ma, T. Y., Gao, G., Du, X.-W., and Qiao, S. Z. (2015). Porous P-Doped Graphitic Carbon Nitride Nanosheets for Synergistically Enhanced Visible-Light Photocatalytic H<sub>2</sub> Production. *Energy Environ. Sci.* 8, 3708–3717. doi:10.1039/c5ee02650d
- Santosa, S. J., Siswanta, D., Sudiono, S., and Utarianingrum, R. (2008). Chitin-Humic Acid Hybrid as Adsorbent for Cr(III) in Effluent of Tannery Wastewater Treatment. *Appl. Surf. Sci.* 254, 7846–7850. doi:10.1016/j.apsusc.2008.02.102
- Shi, A., Li, H., Yin, S., Hou, Z., Rong, J., Zhang, J., et al. (2018). Photocatalytic NH<sub>3</sub> Versus H<sub>2</sub> Evolution Over g-C<sub>3</sub>N<sub>4</sub>/C<sub>54</sub>WO<sub>3</sub>:O<sub>2</sub> and Methanol Tipping the Scale. *Appl. Catal. B Environ.* 235, 197–206. doi:10.1016/j.apcatb.2018.04.081
- Sun, D., Ban, R., Zhang, P.-H., Wu, G.-H., Zhang, J.-R., and Zhu, J.-J. (2013). Hair Fiber as a Precursor for Synthesizing of Sulfur- and Nitrogen-Co-Doped Carbon Dots with Tunable Luminescence Properties. *Carbon* 64, 424–434. doi:10.1016/j.carbon.2013.07.095
- Tan, J., Zou, R., Zhang, J., Li, W., Zhang, L., and Yue, D. (2016). Large-Scale Synthesis of N-Doped Carbon Quantum Dots and Their Phosphorescence Properties in a Polyurethane Matrix. *Nanoscale* 8, 4742–4747. doi:10.1039/c5nr08516k
- Tasbihi, M., Fresno, F., Simon, U., Villar-García, I. J., Pérez-Dieste, V., Escudero, C., et al. (2018). On the Selectivity of CO<sub>2</sub> Photoreduction towards CH<sub>4</sub> Using Pt/TiO<sub>2</sub> Catalysts Supported on Mesoporous Silica. *Appl. Catal. B Environ.* 239, 68–76. doi:10.1016/j.apcatb.2018.08.003
- Wang, P., Yi, X., Lu, Y., Yu, H., and Yu, J. (2018). In-Situ Synthesis of Amorphous H<sub>2</sub>TiO<sub>3</sub>-Modified TiO<sub>2</sub> and its Improved Photocatalytic H<sub>2</sub>-Evolution Performance. *J. Colloid Interface Sci.* 532, 272–279. doi:10.1016/j.jcis.2018.07.139
- Xia, J., Di, J., Li, H., Xu, H., Li, H., and Guo, S. (2016). Ionic Liquid-Induced Strategy for Carbon Quantum dots/BiOX (X = Br, Cl) Hybrid Nanosheets with Superior Visible Light-Driven Photocatalysis. *Appl. Catal. B Environ.* 181, 260–269. doi:10.1016/j.apcatb.2015.07.035
- Xiao, J.-D., and Jiang, H.-L. (2017). Thermally Stable Metal-Organic Framework-Templated Synthesis of Hierarchically Porous Metal Sulfides: Enhanced Photocatalytic Hydrogen Production. *Small* 13, 1700632. doi:10.1002/smll.201700632
- Yan, T., Tian, J., Guan, W., Qiao, Z., Li, W., You, J., et al. (2017). Ultra-Low Loading of Ag<sub>3</sub>PO<sub>4</sub> on Hierarchical In<sub>2</sub>S<sub>3</sub> Microspheres to Improve the Photocatalytic Performance: The Cocatalytic Effect of Ag and Ag<sub>3</sub>PO<sub>4</sub>. *Appl. Catal. B Environ.* 202, 84–94. doi:10.1016/j.apcatb.2016.09.017
- Yang, B., Lv, K., Li, Q., Fan, J., and Li, M. (2019). Photosensitization of Bi<sub>2</sub>O<sub>2</sub>CO<sub>3</sub> Nanoplates with Amorphous Bi<sub>2</sub>S<sub>3</sub> to Improve the Visible Photoreactivity

- towards NO Oxidation. *Appl. Surf. Sci.* 495, 143561. doi:10.1016/j.apsusc.2019.143561
- Yang, F., Liao, C., Wang, M., Zheng, B., Xiao, D., Wu, L., et al. (2018). One-Step Synthesis of N/P-Doped Carbon Dots and Their Fluorescence Properties. *Chem. Res. Appl.* 30, 313. doi:10.3969/j.issn.1004-1656.2018.03.001
- Yu, H., Shi, R., Zhao, Y., Waterhouse, G. I. N., Wu, L.-Z., Tung, C.-H., et al. (2016). Smart Utilization of Carbon Dots in Semiconductor Photocatalysis. *Adv. Mat.* 28, 9454–9477. doi:10.1002/adma.201602581
- Zhang, H., Huang, H., Ming, H., Li, H., Zhang, L., Liu, Y., et al. (2012). Carbon Quantum dots/Ag<sub>3</sub>PO<sub>4</sub> Complex Photocatalysts with Enhanced Photocatalytic Activity and Stability under Visible Light. *J. Mat. Chem.* 22, 10501. doi:10.1039/c2jm30703k
- Zhang, N., Li, L., and Li, G. (2017). Nanosized Amorphous Tantalum Oxide: A Highly Efficient Photocatalyst for Hydrogen Evolution. *Res. Chem. Intermed.* 43, 5011–5024. doi:10.1007/s11164-017-3052-y
- Zhou, Y., Lv, P., Zhang, W., Meng, X., He, H., Zeng, X., et al. (2018). Pristine Bi<sub>2</sub>WO<sub>6</sub> and Hybrid Au-Bi<sub>2</sub>WO<sub>6</sub> Hollow Microspheres with Excellent Photocatalytic Activities. *Appl. Surf. Sci.* 457, 925–932. doi:10.1016/j.apsusc.2018.07.024

**Conflict of Interest:** Author HJ was employed by Zhejiang Hongyi Environmental Protection Technology Co., Ltd. Authors YW and XZ were employed by

Environmental Engineering Corporation of Zhejiang Province. Author DM was employed by Zhejiang Tianchuan Environmental Science and Technology Co., Ltd.

The remaining authors declare that the research was conducted in the absence of any commercial or financial relationships that could be construed as a potential conflict of interest.

**Publisher's Note:** All claims expressed in this article are solely those of the authors and do not necessarily represent those of their affiliated organizations, or those of the publisher, the editors, and the reviewers. Any product that may be evaluated in this article, or claim that may be made by its manufacturer, is not guaranteed or endorsed by the publisher.

Copyright © 2022 Li, Qiu, Jin, Wang, Ma, Zhang, Yang and Wang. This is an open-access article distributed under the terms of the Creative Commons Attribution License (CC BY). The use, distribution or reproduction in other forums is permitted, provided the original author(s) and the copyright owner(s) are credited and that the original publication in this journal is cited, in accordance with accepted academic practice. No use, distribution or reproduction is permitted which does not comply with these terms.